Relativistic distorted-wave procedures with pseudostates

Guo-Xin Chen
ITAMP, Harvard-Smithsonian Center for Astrophysics, 60 Garden Street, Cambridge, Massachusetts 02138, USA
(Received 23 November 2007; published 1 February 2008)

The relativistic distorted-wave (RDW) procedures developed by Chen [Phys. Rev. A **53**, 3227 (1996)] have been extended to include pseudostates. The RDW procedures with pseudostates are applied to the calculation of electron impact excitation (EIE) of Fe XVII. Pseudostates are shown to have a significant effect on the cross sections for important transitions such as $3C$ ($\lambda=15.015$ Å) and $3D$ ($\lambda=15.262$ Å) of Fe XVII. The convergence of the RDW calculations has been carefully investigated. The present RDW calculations of Fe XVII are further compared with our previous close coupling results using the fully relativistic Dirac *R*-matrix (DRM) method, where resonance and more complete channel coupling effects were included in addition to the background direct excitations. The present RDW calculations are in good agreement to the background cross sections from the DRM calculations. This agreement indicates the mutual confirmation of the validity of both the RDW and the DRM calculations of the direct or background EIE cross sections.

DOI: 10.1103/PhysRevA.77.022701 PACS number(s): 34.80.−i

I. INTRODUCTION

In addition to the basic research interest, the study of fundamental atomic processes such as electron impact excitation (EIE), electron impact ionization, photoionization, and photorecombination has long been driven by important applications to astrophysical, fusion, and laser-produced plasmas [1–4]. The calculations of these radiative and collisional atomic processes are essential for theoretical modeling and diagnostics of plasmas, such as the accurate determination of element abundances and level population [5–8] in astrophysical plasmas of photoionized equilibrium or collisionally ionized equilibrium, appearing in solar and stellar coronae, active galactic nuclei, supernovae, and black holes [9–11].

For highly charged ions (HCI) often showing up in high-temperature hot plasmas, the relativistic distorted-wave (RDW) method may be of some use to study EIE and other atomic processes. The relativistic effects in both the atomic structure and the collision dynamics may be significant for EIE scattering processes in HCI. The RDW method with the input of relativistic atomic structure is suitable to include fully relativistic effects in target atomic structure and collision dynamics. There are several variants of the RDW method, but as far as channel coupling is concerned, the assumption is that the inclusion of the initial and final channels may be sufficient for the calculation of the scattering matrix elements. The basic feature in the RDW method is that within the framework of the Kohn variational principle the coupling between scattering channels is weak [12]. This approximation may reduce a set of integrodifferential (ID) equations to a procedure of solving a single ID or mainly a differential equation to allow for the distortion of the wave function which describes the inelastically scattered electron.

Another important RDW feature is that RDW allows for the distortion of the channel wave functions in the target distortion potential from their asymptotic Coulomb form. We will address below some approximations of the exchange distortion potential used in RDW and the validity of RDW for HCI. The general criterion for the validity of the RDW method is that the absolute value of the reactance matrix element $|K_{ij}| \ll 1$, a condition that may be satisfied for HCI since $|K_{ij}|$ scales as $Z_{\mathrm{eff}}^{-1}=(Z-N)^{-1}$ (Z is the nuclear charge and N is the electron number in the target ion). For HCI, the RDW theory may be comparable to the relativistic Dirac *R*-matrix (DRM) theory [13] or the Breit-Pauli *R*-matrix (BPRM) theory [14], both of which have been used in our previous investigation of EIE of Fe XVII and other ions [6,15–18]. Both the DRM and the BPRM close-coupling (CC) methods can be time consuming in computation, while the RDW method stands out to be efficient in computation. For HCI, the RDW method may be sufficiently accurate to cross check the background or direct cross sections in DRM or BPRM calculations. Some comparative study of the RDW and DRM calculations of EIE of Ne IX has recently been carried out in Ref. [17].

Since the 1980s, a number of RDW codes have been developed (e.g., Refs. [19–21]). These codes have been widely used for EIE calculations of a range of atomic ions. I have also developed an accurate and efficient RDW code [22] in 1996 to calculate EIE cross sections of HCI using the relativistic atomic structure code GRASP [23]. My RDW code was then extended to use the relativistic atomic structure code GRASP2 [24] as the target calculation input [25–27]. There are some elaborate procedures considered in my RDW code such as the the accurate calculation of continuum electron wave functions. I have also investigated the effects of different types of distortion potentials using my RDW code [26,27]. We consider the RDW method as a two-state close coupling (2CC) approximation [12], so our RDW method may take into account the distortion of the incident and scattered waves by different distortion potentials.

In this work, I extend the procedures in my RDW code to include pseudostates. As a case study, my RDW code with the inclusion of pseudostates is then used to calculate EIE collision strengths of Fe XVII x-ray transitions $3C$ ($\lambda=15.015$ Å, $2p^5 3d\ ^1P_1^o \rightarrow 2p^6\ ^1S_0$) and $3D$ ($\lambda=15.262$ Å, $2p^5 3d\ ^3D_1^o \rightarrow 2p^6\ ^1S_0$), important for applications to astrophysics and EBIT (electron beam ion trap) science [5,6,15,16,28]. There is currently a plethoric theoretical and experimental study of Fe XVII atomic and spectral systems

[28–31,15,16]. Because Fe XVII is a HCI with large fractional abundance in a variety of plasmas, the $3C$ and $3D$ lines and some other x-ray lines in the range of 10–17 Å in Fe XVII are prominent and may be used as fundamental spectral and abundance diagnostics [5,6,15,16]. In this work, I carry out some elaborate and consistent RDW calculations of EIE of Fe XVII with and without pseudostates in order to demonstrate the effects of pseudostates and the convergence of RDW calculations. Furthermore, the present RDW calculations of $3C$ and $3D$ cross sections with and without pseudostates are, respectively, compared with my previous DRM results [15] also with and without pseudostates, in order to cross check and mutually validate both calculations.

This paper is structured as follows. In Sec. II the RDW method is outlined. The RDW computation modes for EIE of Fe XVII are given in Sec. III. The results from the RDW calculations of EIE of Fe XVII are presented in Sec. IV. Finally, in Sec. V a brief summary is given.

II. OUTLINE OF THE RDW METHOD

I outline the RDW method in this section in order to explicitly show the extension of the RDW procedures to the inclusion of pseudostates. More details of the procedures built in my RDW code, especially for the special techniques on the solution and normalization of continuum wave functions and for the top-up procedures of high-partial-wave collision strengths, should be referred to our earlier separated publications and references therein [22,25–27].

A. Relativistic bound and continuum wave function

We use the N- and $(N+1)$-electron Dirac-Coulomb (DC) Hamiltonian to describe the target ion and the collisional atomic system, respectively. The DC Hamiltonian in Rydberg units for electrons i and j in a central field Z (atomic number $Z=26$ for Fe XVII) can be written as

$$H^{\mathrm{DC}} = \sum_{i=1} \left(\boldsymbol{\alpha}\cdot\boldsymbol{p}_i/\alpha + \beta/\alpha^2 - \frac{2Z}{r_i} + \sum_{j>i}\frac{2}{r_{ij}} \right), \tag{2.1}$$

where the quantities $\boldsymbol{\alpha}$ and β are the Dirac matrices in the low-energy representation and $\alpha=1/137.036$ is the fine-structure constant. The total wave functions for a given symmetry $J\Pi$ (J is the total angular momentum in a jj-coupling scheme and Π is the parity) are constructed from bound $[\phi_{n\kappa m}(\boldsymbol{r})]$ and free $[\theta_{\epsilon\kappa m}(\boldsymbol{r})]$ Dirac four-component spinors

$$\phi_{n\kappa m}(\boldsymbol{r}) = \langle r|n\kappa m\rangle = \frac{1}{r}\begin{bmatrix} P_{n\kappa}(r) & \chi_{\kappa m}(\boldsymbol{r}/r) \\ \mathrm{i}\, Q_{n\kappa}(r) & \chi_{-\kappa m}(\boldsymbol{r}/r) \end{bmatrix}, \tag{2.2}$$

$$\theta_{\epsilon\kappa m}(\boldsymbol{r}) = \langle r|\epsilon\kappa m\rangle = \frac{1}{r}\begin{bmatrix} P_{\epsilon\kappa}(r) & \chi_{\kappa m}(\boldsymbol{r}/r) \\ \mathrm{i}\, Q_{\epsilon\kappa}(r) & \chi_{-\kappa m}(\boldsymbol{r}/r) \end{bmatrix}, \tag{2.3}$$

where $P_{n\kappa}$ ($P_{\epsilon\kappa}$) and $Q_{n\kappa}$ ($Q_{\epsilon\kappa}$) are the large- and small-component of the bound (free) radial wave functions, respectively. The function $\chi_{\kappa m}$ is the spinor spherical harmonic

$$\chi_{\kappa m}(\boldsymbol{r}/r) = \sum_{\delta=\pm\frac{1}{2}} \left\langle lm-\delta\tfrac{1}{2}\delta \middle| l\tfrac{1}{2}jm \right\rangle \mathrm{Y}_l^{m-\delta}(\vartheta,\varphi)\phi^{\delta}, \tag{2.4}$$

where $\langle lm-\delta\frac{1}{2}\delta|l\frac{1}{2}jm\rangle = C(lm-\delta\frac{1}{2}\delta;jm)$ is a Clebsch-Gordan coefficient; $\mathrm{Y}_l^{m-\delta}(\vartheta,\varphi)$ is a spherical harmonic; ϕ^{δ} is a spinor basis function. The relativistic angular quantum number $\kappa=-(j+1/2)a$ for $l=j-1/2a$ ($a=\pm 1$), and the total angular momentum of a single electron $j=|\kappa|-1/2$. m and δ are the magnetic quantum numbers along some arbitrary projection axis for the orbital angular momentum l and the spin of the bound or free electron, respectively. Because the Hamiltonian H^{DC} is invariant with respect to the rotational reference frame, its N-electron eigenfunctions with the same energy E and parity Π can be used to construct a product representation of the rotation group SO(3) which is usually reducible. The set of states $\{n\kappa m|m=-j,-j+1,\ldots,+j\}$ spans an irreducible four-spinor representation $D^{(j)}$ of the SO(3) group [32].

The bound electron wave functions and atomic structure are calculated by the multi-configuration Dirac-Fock (MCDF) method which is a self-consistent-field (SCF) procedure and both the orbitals and the configuration expansion coefficients are variationally determined [23,24]. The GRASP2 code has been significantly modified as the input of the target structure calculation to our RDW code [24]. In the linear configuration expansion (CE) approach built within the MCDF framework, the atomic state functions (ASF) $\Psi_m = |\Gamma JM\rangle$ are a linear combination of configuration state function (CSF) $\Phi_i = |\gamma JM\rangle$ sharing common values of the total angular momentum J and M, and the parity Π,

$$\Psi_m = \sum_{i=1}^{n_{\mathrm{C}}} C_{im}\Phi_i, \quad m=1,\ldots,n_{\mathrm{A}}, \tag{2.5}$$

where C_{im} are the mixing coefficients; n_{C} and n_{A} are the number of SCF and ASF, respectively. A CSF may be constructed from the products of one-electron spinors in a system of N electrons (the Slater determinant). The major extension of the RDW procedures as presented in this work is to include pseudostates in the linear configuration expansion equation (2.5).

We determine the Dirac free spinor $\theta_{\epsilon\kappa m}$ (distorted-wave) for a free electron in the distortion potential $V(r)$ (which is a spherically symmetric central potential) due to the target ion. The large and small components $P_{\epsilon\kappa}$ and $Q_{\epsilon\kappa}$ of the continuum electron orbital satisfy the coupled Dirac equations

$$\left[\frac{d}{dr}+\frac{\kappa}{r}\right]P_{\epsilon\kappa}(r) = \frac{\alpha}{2}[\epsilon - V(r) + 4/\alpha^2]Q_{\epsilon\kappa}(r),$$

$$\left[\frac{d}{dr}-\frac{\kappa}{r}\right]Q_{\epsilon\kappa}(r) = -\frac{\alpha}{2}[\epsilon - V(r)]P_{\epsilon\kappa}(r), \tag{2.6}$$

where the kinetic energy of the free electron ϵ (in Ry) is positive. The solution of the free electron orbitals play a key role in the RDW framework. Some special recipes on the solution of continuum wave functions and continuum

asymptotic normalization in my RDW code should be referred to my earlier paper [22]. The relation between the relativistic wave quantum number k of the impact electron and its relativistic momentum p and kinetic energy ϵ (in Ry) of the impact electron is given by

$$k^2 = \frac{p^2 a_0^2}{\hbar} = \epsilon\left(1 + \frac{\alpha^2}{4}\epsilon\right), \tag{2.7}$$

where a_0 is the Bohr radius. The radial functions for bound and continuum orbitals satisfy the following orthonormality conditions:

$$\int_0^\infty dr[P_{n\kappa}(r)P_{n'\kappa}(r) + Q_{n\kappa}(r)Q_{n'\kappa}(r)] = \delta_{nn'}, \tag{2.8}$$

$$\int_0^\infty dr[P_{\epsilon\kappa}(r)P_{\epsilon'\kappa}(r) + Q_{\epsilon\kappa}(r)Q_{\epsilon'\kappa}(r)] = \pi\delta(\epsilon - \epsilon'), \tag{2.9}$$

where $\delta_{nn'}$ is a Kronecker delta.

B. Relativistic distortion potential

The RDW distortion potential $V(r)$ is used to distort the wave function of the free electron. It is important to choose carefully a suitable distortion potential so that the main feature in an EIE process can be reflected in the free electron wave function, e.g., the relativistic dynamics of free electrons and the coupling between the free electron and the target bound electrons. The distortion potential $V(r)$ may be divided into the direct distortion potential $V^d(r)$ and the exchange distortion potential $V^e(r)$,

$$V(r) = V^d(r) + V^e(r), \tag{2.10}$$

$$V^d(r) = -\frac{2Z(r)}{r} + V_c(r). \tag{2.11}$$

Finite nuclear charge $Z(r)$, which differs from ordinary Z only for small r, is chosen to be the Fermi charge distribution. $Z(r)$ as a function of r can be obtained from the GRASP2 code [23,24].

The residual potential $U(r)$ given below,

$$U(r) = -\frac{2Z(r)}{r} + \sum_{i=1}^{N}\frac{2}{|\boldsymbol{r} - \boldsymbol{r}_i|} - V(r)$$

$$= \sum_{i=1}^{N}\frac{2}{|\boldsymbol{r} - \boldsymbol{r}_i|} - [V_c(r) + V^e(r)], \tag{2.12}$$

is used as a perturbation potential for the subsequent RDW calculation of the transition matrix $\mathbf{T}$ in Eq. (2.15) or the reactance matrix $\mathbf{K}$ in Eq. (2.17). $\mathbf{r}_i$ $(i=1,\ldots,N)$ are the radii of the N bound electrons.

The direct distortion potential $V^d(r)$ is the spherical average of the electron-electron interactions in an $(N+1)$-electron ion. $V_c(r)$ is the spherically averaged classical potential for the free electron in the field of all N electrons of the ion. The exchange distortion potential $V^e(r)$ used for solving free electron orbitals is chosen to be one of the four types of exchange distortion potentials as given in Refs. [26,33] based upon the free-electron gas model: namely, the semiclassical exchange (SCE) potential, the second-order free electron gas exchange (SOFEGE) potential, the asymptotically adjusted free electron gas exchange (AAFEGE) potential, and the Dirac-Fock-Slater (DFS) potential. We have investigated the effects of these four different exchange distortion potentials on RDW calculations of EIE of B II in Ref. [26].

In the present work, we also investigate the effects of the four different exchange distortion potentials on the RDW calculations of EIE of Fe XVII. However, only the SCE potential is chosen in the further RDW calculations for comparisons either between the present different RDW modes or with previous DRM results. The SCE potential depends on the free electron energy so it might be more appropriately used to describe the dynamical EIE process. The DFS potential does not depends on the energy of free electron and it is widely used in previous RDW calculations [20]. It is somehow more convenient to construct a common DFS potential under which the continuum orbitals may be solved to be orthogonal automatically with each other and with the bound electron orbitals.

In my RDW procedures, MCDF potentials from the GRASP2 code are used for bound four-spinor calculations. In this work, we consider the SCE potential physically more plausible, so unless otherwise stated, the SCE potential is used in our RDW calculations of free electron radial orbitals throughout this paper. Since the MCDF and SCE potentials used in the calculations of the bound and free orbitals are different, the free electron orbitals are not orthogonal to those of the bound electrons. More discussions were given in my earlier paper [27], regarding the approximations we have made (due to the fact that the two potentials MCDF and SCE are different), for the calculations of reactance matrix elements.

C. The partial wave expansion

It is often convenient to express the cross section $\sigma_{if}(\epsilon)$ for a transition $i \to f$ in terms of collision strength $\Omega_{if}(\epsilon)$,

$$\sigma_{if}(\epsilon) = \frac{\pi a_0^2}{k_i^2 g_i}\Omega_{if}(\epsilon), \tag{2.13}$$

where k_i is the relativistic wave number of the impact electron and $g_i = [J_i] = 2J_i + 1$ is the statistical weight of the initial state of the N-electron target ion. For a target specified in previous subsection, electron collision processes can be calculated using a partial-wave (PW) expansion with radial functions obtained from the $(N+1)$-electron DC Hamiltonian in Eq. (2.1). Using the PW approach for the colliding electron, the total collision strength Ω is the sum of partial collision strengths Ω^J computed from the transition matrix $\mathbf{T}$ or the reactance matrix $\mathbf{K}$,

$$\Omega_{if}(\epsilon) = \sum_J \Omega_{if}^J(\epsilon), \tag{2.14}$$

$$\Omega_{if}^{J}(\epsilon) = \frac{1}{2}\sum_{\kappa\kappa'} [J]|T(\Gamma_i J_i \kappa J; \Gamma_f J_f \kappa' J)|^2, \qquad (2.15)$$

where $[J]=2J+1$, $T(\Gamma_i J_i \kappa J; \Gamma_f J_f \kappa' J)$ are the transition matrix elements; Γ_i and Γ_f refer to suppressed additional quantum numbers required to specify the pure jj-coupled initial and final states, respectively; J_i and J_f refer to the total angular momenta of the target ion in a certain transition; κ and κ' refer to the total angular momenta of the continuum orbital. For HCI of interest here, we may express the **T** matrix in terms of the reactance matrix **K**:

$$\mathbf{T} = \frac{i\mathbf{I}+\mathbf{K}}{i\mathbf{I}-\mathbf{K}} - \mathbf{I} = \frac{2i\mathbf{K}}{1-i\mathbf{K}} \simeq 2i\mathbf{K}, \qquad (2.16)$$

where the final approximation gives nonunitarization cross section. This is a weak coupling approximation and gives a reasonable treatment for HCI for which the matrix elements of **K** are small. The collision strength is then be expressed in terms of the reaction matrix **K**,

$$\Omega_{if} = 2\sum_{J} [J]\sum_{\kappa\kappa'} |K(\Gamma_i J_i \kappa J; \Gamma_f J_f \kappa' J)|^2. \qquad (2.17)$$

The RDW method may be considered as a two state close coupling (2CC) approximation in the CC or DRM method, so certain amount of direct channel coupling effects may be included in the RDW method. Of course, the remaining channel coupling effects (and interacting Rydberg series of resonances) cannot be treated and are missing in the RDW method. These effects may have to be calculated by the more sophisticated CC or DRM method. However, if the direct channel coupling effects dominate over the indirect channel coupling effects, RDW may be adequately used to calculate the direct or background cross sections.

III. CALCULATION

In this work, I carry out seven sets of RDW calculations for EIE of Fe XVII. In these calculations, Fe XVII target wave functions up to principal quantum number $n=6$ and relativistic angular quantum number $|\kappa|$ up to 5 (or the total angular momentum j up to 9/2) for the singly excited electron from the $2s$ or $2p$ subshell are calculated using the MCDF method [N-electron DC Hamiltonian in Eq. (2.1)]. The purpose of these seven sets of RDW calculations is (a) to show the influence of long-range collisional coupling and correlation effects by the inclusion of pseudostates and (b) to demonstrate the convergence of the present RDW calculations either with or without the inclusion of pseudostates. Because consistent calculations are carried out by the same RDW code, we may make a more meaningful comparison either between the present different computation modes or between the present and previous RDW results. Furthermore, the present RDW results may also be of some use to elucidate previous similar calculations by different methods or codes.

In the first calculation (A) (referred to as mode $n=3$ below), target states up to $n=3$ in $2s^2 2p^6$ and $2s^2 2p^5 3l$ ($l=s,p,d$) are included. In the second calculation (B) (mode $n=4$), in addition to (A), I include $2s^1 2p^6 3l$ ($l=s,p,d$), and $2s^2 2p^5 4l$ and $2s^1 2p^6 4l$ ($l=s,p,d,f$). In the third calculation (C) (mode $n=5$), I add $2s^2 2p^5 5l$ ($l=s,p,d,f,g$) to (B). In the fourth calculation (D) (mode $n=6$), I add $2s^2 2p^5 6l$ ($l=s,p,d,f,g$) to (C). In the fifth calculation (E) (mode $n=5+$), in addition to those states in (C), I include the configuration $2s^2 2p^4 3d^2$ to reflect the pair excitation effects (or pair correlation effects) from the ground configuration $2s^2 2p^6$; I also include pseudo-orbitals with the relativistic angular quantum number $|\underline{\kappa}|=1-3$ to incorporate the short-range exchange effects and the long-range correlation and collisional coupling effects. To show the convergence of calculation (E), I also carry out two further calculation modes (F) (mode $n=4+$) and (G) (mode $n=6+$), adding the pair excitation configuration and the pseudo-orbitals mentioned in (E) to (B) and (D), respectively.

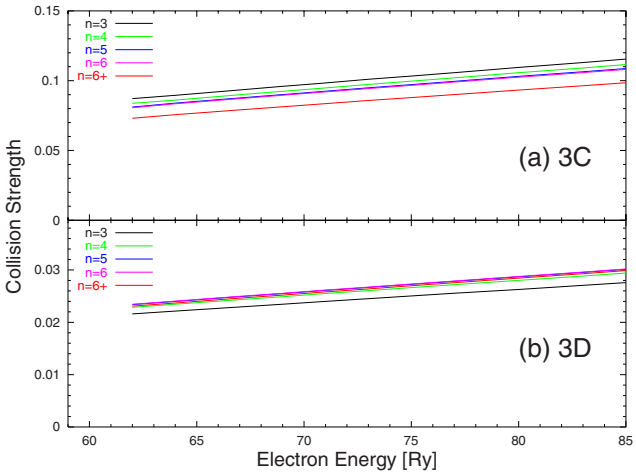

FIG. 1. (Color online) Collision strengths Ω as a function of incident electron energy ϵ for $3C$ [top panel (a)] and $3D$ [bottom panel (b)] transitions of Fe XVII. For panel (a) from top to bottom: black (mode $n=3$); green (mode $n=4$) (thin grey in black and white printing); blue (mode $n=5$) (black); orange (mode $n=6$) (thin grey); red (mode $n=6+$) (thick grey). The color is the same for bottom panel.

IV. RESULT

A. Convergence and pseudostate effects

To show the effects of pseudostates and the convergence in my RDW calculations of EIE of Fe XVII, I present the collision strengths Ω from five different computation modes for $3C$ and $3D$ transitions in Fig. 1. We use mode $n=3$ (thick black line) as the "baseline" for comparisons. For the $3C$ transition, the effects of pseudostates in mode $n=6+$ are shown to be important (with a 10–20% reduction) when compared with Ω from the $n=3$ "baseline" mode and other modes. Without pseudostates, while the mode $n=5$ improves slightly over the mode $n=4$, we find that the mode $n=6$ shows little improvement over the mode $n=5$ for the $3C$ transition. This further demonstrates the importance of the inclusion of pseudostates in mode $n=6+$. The results from $n=4+$ and $n=5+$ modes are converged to the $n=6+$ mode, so both modes are not shown in Fig. 1. The results from modes

TABLE I. Cross sections σ (in units 10^{-19} cm^2=0.1 Mb) for $3C$ and $3D$ transitions of Fe XVII from the present RDW calculations are compared with previous results.

	ϵ (eV)		converged calc.							previous calc.		Expt.
			$n=3$	4	5	6	4+	5+	6+	[20]	[30]	[30]
$3C$	910	RDW	1.23	1.18	1.15	1.14	1.03	1.04	1.04	1.21	1.26	0.849 ± 0.16
		DRM	1.24	1.25	1.19		1.08	1.06	1.06[a]			
	964	RDW	1.22	1.17	1.15	1.14	1.02	1.03	1.03	1.19	1.30	0.888 ± 0.93
		DRM	1.23	1.26	1.21		1.08	1.06	1.07[a]			
$3D$	910	RDW	0.301	0.319	0.327	0.328	0.323	0.323	0.323	0.319	0.417	0.310 ± 0.64
		DRM	0.312	0.403	0.385		0.394	0.383	0.384[a]			
	964	DRM	0.297	0.316	0.323	0.324	0.319	0.320	0.320	0.314	0.437	0.298 ± 0.33
		DRM	0.308	0.394	0.390		0.385	0.381	0.391[a]			

[a]DRM calculations from mode $n=5+$ with the inclusion of cascade effects, dubbed as mode $n=5++$ in Ref. [15].

$n=4+$ and $n=5+$ are given in Table I below. In Fig. 1(a), from the comparison between curves of mode $n=6+$ and other curves, we find that it is important to include the pair excitation configuration and the pseudostates (for the long-range correlation and collisional coupling effects) for the $3C$ transition. For the $3D$ transition, all the modes $n=4-6$ and the modes $n=4+$ to 6+ appear to converge and they are about 8% larger than the "baseline" results from mode $n=3$. Because of the competition of these different effects mainly from the target correlation effects and the collisional coupling effects, the combined effects with the pseudostates and the pair excitation configuration in modes $n=4+$—6+ are small for the $3D$ transition.

In Table I, the cross sections from all the present seven calculation modes are listed to compare in order to further demonstrate the convergence in the present RDW results and to show the effects of the pseudostates and the pair excitation configuration. Our calculations are also compared with the previous theory and experiment results in Table I. The DRM results shown in Table I are in fact the effective cross sections defined in Ref. [15]. The results of mode $n=3$ should be comparable to those in Ref. [34]. The RDW results [20] without resonances and cascades are similar to mode $n=4$ results as evidenced from Table I. The tenth column in the DRM entry is for the DRM calculations of mode $n=5+$ with the inclusion of cascade effects, dubbed as mode $n=5++$ in Ref. [15]. These DRM data in the tenth column should be comparable to the electron beam ion trap (EBIT) results [30] and the RDW results in [30] (last two columns), both of which include the cascade and resonance effects. But the resonance effects in the RDW calculation presented in Ref. [30] may not be as accurate as my previous DRM results. In fact, the comparison of my DRM calculations of mode $n=5+$ with the EBIT and the RDW data given in Ref. [30] (last two columns) has been extensively and deeply discussed in my previous paper [15].

From Fig. 1 and Table I, we find that the convergence of target correlation and collisional coupling is achieved in modes $n=4+$—6+. The difference between the present RDW results and my previous DRM calculations with the same calculation modes clearly shows the importance of resonance effects that were included in my previous DRM calculations but are not in the present RDW calculations. The effects of resonances are much more pronounced in the $3D$ transition than in the $3C$ transition as expected.

For the $3C$ transition, the RDW cross sections σ from mode $n=6+$ (10th column) are 11% smaller than those from mode $n=6$ (7th column). This fact demonstrates the importance of the inclusion of pseudostates and the pair correlation configuration in mode $n=6+$. For the $3D$ transition, the RDW σ of mode $n=6+$ are only slightly different from the σ of mode $n=6$ due to the competition between the target correlation and the collisional coupling effects as explained above. In a separated check, the mode $n=6+$ cross sections are compared with the results when the pair excitation configuration is removed from mode $n=6+$. We find that the effects of the pair excitation configuration reduce the $3C$ and $3D$ cross sections by 4 and 2 %, respectively.

In Table II, I compare the RDW and DRM calculations for a range of of impact electron energies for modes $n=5$ and $n=5+$. For the $3C$ transition, the resonance effects enhance the DRM results by up to 5% when compared with the corresponding RDW data with the same computation mode (n.b.

TABLE II. Cross sections σ (in units 10^{-19} cm^2=0.1 Mb) for $3C$ and $3D$ transitions of Fe XVII between the present RDW calculations and our previous DRM calculation [15] for modes $n=5$ and $n=5+$.

	mode	method	ϵ (eV)				
			840	870	910	964	2000
$3C$	$n=5$	RDW	1.15	1.15	1.15	1.15	1.00
		DRM	1.15	1.20	1.19	1.21	0.991
	$n=5+$	RDW	1.04	1.04	1.04	1.03	0.913
		DRM	1.02	1.07	1.06	1.06	0.887
$3D$	$n=5$	RDW	0.332	0.330	0.327	0.323	0.269
		DRM	0.369	0.409	0.385	0.390	0.267
	$n=5+$	RDW	0.328	0.325	0.323	0.320	0.269
		DRM	0.364	0.410	0.383	0.381	0.271

TABLE III. Cross sections σ (in units 10^{-19} cm^2=0.1 Mb) for $3C$ and $3D$ of Fe XVII from the present mode n=5+ RDW calculations with four types of exchange distortion potentials.

	ϵ(eV)	exchange distortion potential				
		SCE	SOFEGE	AAFEGE	DFS	DRM
$3C$	840	1.04	1.06	1.09	1.07	1.02
	870	1.04	1.06	1.08	1.07	1.07
	910	1.04	1.06	1.07	1.07	1.06
	964	1.03	1.05	1.06	1.06	1.06
	2000	0.913	0.913	0.915	0.923	0.887
$3D$	840	0.328	0.334	0.340	0.335	0.364
	870	0.325	0.331	0.335	0.333	0.410
	910	0.323	0.328	0.331	0.330	0.383
	964	0.320	0.324	0.326	0.327	0.381
	2000	0.269	0.269	0.270	0.272	0.271

for mode n=5+ the DRM value of 0.887 in unit 0.1 Mb at 2000 eV is 3% smaller than the RDW value of 0.913); for the $3D$ transition, the DRM results are up to 25% larger. This is again a strong indication of resonance effects that are not included in the present RDW calculations. Furthermore and more importantly, we find that the difference between the RDW and DRM results varies with electron energies. This interesting feature indicates that the effects of resonance enhancement are *not* uniformly appearing in the resonance region of both $3C$ and $3D$ transitions. The mode n=5+ results for the $3C$ transition in Table II are about 11% smaller than the mode n=5 data, for a wider range of impact energies than in Table I. This is because the inclusion of pseudostates and the pair correlation configuration in mode n=5+, as we already explain above. However, when a similar comparison is made for the $3D$ transition between modes n=5 and n=5+, we find that for the full range of impact energies in Table II there is a rather small difference for the $3D$ transition due to the competition of different effects.

B. Effects of exchange distortion potential

In Table III, we investigate the effects of four types of different exchange distortion potentials, as discussed in Sec. II B and given in Ref. [26]. The DRM data are shown in the last column for a baseline comparison. Generally, there is an overall agreement between the RDW results with the four different distortion potentials. The difference is up to 5% for the $3C$ transition and up to 4% for 3D at low electron energy, where the correlation and exchange effects are expected to have more influence on the RDW cross sections. The different treatments of the correlation and exchange effects are expected to have more influence on the calculations of some ions with lower ionization stages [26]. At high energy, there is hardly any difference among RDW results using different types of exchange distortion potentials.

C. Comparison with background of DRM collision strength

In Figs. 2–5, I compare the present RDW collision strengths with my previous DRM results for modes n=3, 4, 5, and 5+, respectively. The RDW data are in agreement to the backgrounds of the DRM data. This agreement is a strong indication of the mutual validation of both the RDW and DRM calculations. This agreement also shows that the collisional coupling may be adequately taken into account by my RDW code as far as the background or direct cross sections are concerned. Of course, the resonance effects in particular the interacting Rydberg resonance series may not be well treated by the RDW method, as we emphasized in our earlier publications [15–17]. The detailed DRM collision strengths from n=5+ mode have been reported in Ref. [15]. However, the detailed DRM collision strengths with resonance structures from the other three modes (n=3–5) shown in Figs. 2–4 are only first presented in this paper. The DRM calculations from mode n=6 and n=6+ are currently still underway. These calculations have not yet been finished, so

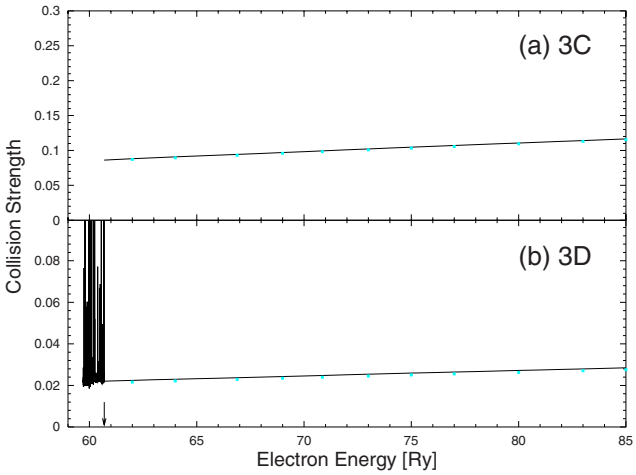

FIG. 2. (Color online) The mode n=3 RDW collision strengths Ω (blue squares) as a function of incident electron energy ϵ for $3C$ [top panel (a)] and $3D$ [bottom panel (b)] transitions of Fe XVII are compared with the background of detailed mode n=3 DRM Ω.

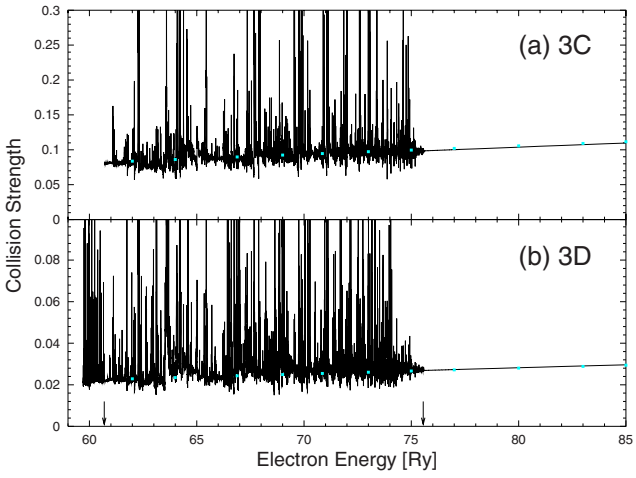

FIG. 3. (Color online) The mode n=4 RDW collision strengths Ω (blue squares) as a function of incident electron energy ϵ for $3C$ [top panel (a)] and $3D$ [bottom panel (b)] transitions of Fe XVII are compared with the background of detailed mode n=4 DRM Ω.

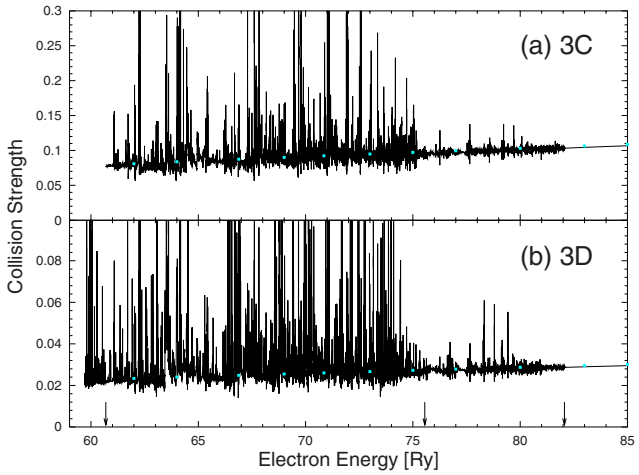

FIG. 4. (Color online) The mode $n=5$ RDW collision strengths Ω (blue squares) as a function of incident electron energy ϵ for $3C$ [top panel (a)] and $3D$ [bottom panel (b)] transitions of Fe XVII are compared with the background of detailed mode $n=5$ DRM Ω.

their results cannot be shown in Table I and here for comparisons.

In Fig. 2, since the highest target threshold included in the $n=3$ mode DRM CC expansion is just the excitation threshold of the $3C$ transition, there is no resonance effects appearing in the $3C$ transition at all. There is a narrow region of resonance enhancement in the $3D$ transition for mode $n=3$, simply due to the slightly smaller excitation energy of the $3D$ transition.

In Fig. 3, by using the mode $n=4$ DRM CC expansion, pronounced resonance features start to show up in both the $3C$ and $3D$ transitions for a range of electron energies up to 75 Ry. In Figs. 4 and 5, with the mode $n=5$ and 5+ DRM CC expansion, the resonance features show up in the region 75–82 Ry. However, the strength of the resonance enhancement is small when compared to that in the region 60–75 Ry. It should be noted that in the mode $n=4$, 5, and 5+ DRM calculations, some broad and diffuse resonance enhancements may be found in the energy range 63–65 Ry and 66.5–68 Ry. These interesting resonance features are due to many interacting Rydberg resonance series appearing in the same energy region. Some similar broad and diffuse resonance features have also been found and deeply investigated in our earlier EIE calculation of Fe^{5+} using the BPRM method [18]. In Fig. 5, the pseudostates and the pair excitation configuration are included in the DRM and RDW calculations. The extensive discussions of DRM calculations in Fig. 5 have already been given in my previous paper [15].

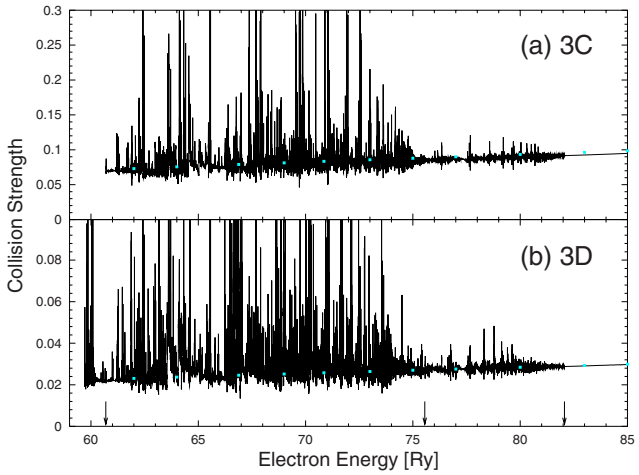

FIG. 5. (Color online) The mode $n=5+$ RDW collision strengths Ω (blue squares) as a function of incident electron energy ϵ for $3C$ [top panel (a)] and $3D$ [bottom panel (b)] transitions of Fe XVII are compared with the background of detailed mode $n=5+$ DRM Ω.

Since RDW calculations may be considered as a 2CC approximation, the agreement, between the RDW $3C$ and $3D$ collision strengths and the backgrounds of the DRM Ω with resonances, as shown in Figs. 2–5, demonstrates that the major part of channel coupling effects may be adequately calculated with our RDW code for $3C$ and $3D$ EIE of Fe XVII. This in turn shows that the direct channel coupling effects dominate over the indirect channel coupling effects for $3C$ and $3D$ cross sections.

V. SUMMARY

A brief summary of the results I have given is presented below.

(1) I have extended my RDW procedures to include pseudostates. The RDW code with pseudostates has been used to calculate the $3C$ and $3D$ EIE cross sections of Fe XVII. The importance of the inclusion of pseudostates in the RDW calculations is demonstrated. The effect of pair correlation configuration $2s^2 2p^4 3d^2$ may reduce the $3C$ and $3D$ collision strengths by a few per cent. The 3C EIE collision strengths may be reduced by as much as 10–15% due to the inclusion of pseudostates and pair correlation configuration. The overall combined effects on 3D is small due to the competition outcome of the different effects, mainly from the correlation effects in the target structure and from the collisional coupling effects.

(2) The effects of different types of distortion potentials on $3C$ and $3D$ cross sections have been investigated. From the comparison of four types of exchange distortion potentials (different free electron gas approximation), the difference may reach 5% at low impact energy. There is no effect at high impact energy.

(3) The convergence in our RDW calculation of EIE of Fe XVII is shown for both cases with and without pseudostates. The RDW results are compared with the background collision strengths in my previous DRM calculations with similar computation modes. Good agreement is found in all the cases that are compared in this work. This agreement is an indication for the mutual validation of both the present RDW calculation and my previous DRM work. This agreement further shows that the direct channel coupling effects dominate over the indirect channel coupling effects for the $3C$ and $3D$ transitions. Our RDW procedures are therefore adequate to be used for the calculation of $3C$ and $3D$ direct or background collision strengths in EIE of Fe XVII.

(4) In both our RDW and DRM procedures for the calcu-

lations of atomic processes, the GRASP2 code is used as atomic structure inputs. These procedures may be of some particular use and benefit to assess the effects of resonance enhancement and channel coupling because the same target structure can be used for further RDW and DRM collisional calculations.

(5) With the inclusion of pseudostates and pair correlation configuration, the accuracy of the present converged RDW calculation for the direct $3C$ and $3D$ collision strengths is shown to be $\approx 5\%$. Due to the overall good agreement (from the cross check) between the RDW and DRM calculations, the accuracy of the background collision strengths of $3C$ and $3D$ transitions in our previous converged DRM calculations is also shown to be $\approx 5\%$.

The fact that a set of highly accurate atomic data for Fe XVII has been completed from this work and my previous DRM work is expected to have an important impact on x-ray astrophysics. The immediate application of the present results to astrophysical, fusion, and laser-produced plasmas is implied. The results obtained and the method used in this paper should have some impact on the general RDW calculations of fundamental atomic processes. A systematic calculation of atomic processes in Ne isoelectronic sequence and other ions is currently underway.

ACKNOWLEDGMENTS

It is a pleasure for the author to thank our EBIT team members at NIST and CfA for stimulating discussions. The author is also grateful for K. Kirby and N.S. Brickhouse's encouragement of the project. This work was supported by NSF through a grant for the Institute for Theoretical Atomic, Molecular and Optical Physics at Harvard University and Smithsonian Astrophysical Observatory and in part by a Chandra X-ray Observatory (CXO) theory grant. The computational work was carried out on the Cluster at the Computation Facility of CfA.

[1] T. R. Kallman and P. Palmeri, Rev. Mod. Phys. **79**, 79 (2007).
[2] G. X. Chen and A. K. Pradhan, Astrophys. J. **536**, 420 (2000).
[3] M. D. Rosen *et al.*, Phys. Rev. Lett. **54**, 106 (1985); D. L. Matthews *et al.*, *ibid.* **54**, 110 (1985).
[4] R. E. Marrs, M. A. Levine, D. A. Knapp, and J. R. Henderson, Phys. Rev. Lett. **60**, 1715 (1988).
[5] B. W. Smith, J. C. Raymond, J. B. Mann, and R. D. Cowan, Astrophys. J. **298**, 898 (1985).
[6] G. X. Chen, K. Kirby, E. Silver, N. S. Brickhouse, J. D. Gillaspy, J. N. Tan, J. Pomeroy, and J. M. Laming, Phys. Rev. Lett. **97**, 143201 (2006).
[7] R. K. Smith, N. S. Brickhouse, D. A. Liedahl, and J. C. Raymond, Astrophys. J. Lett. **556**, L91 (2001).
[8] M. S. Turner *et al.*, *Connecting Quarks with the Cosmos* (National Academies Press, Washington, DC, 2003).
[9] C. R. Canizares *et al.*, Astrophys. J. Lett. **539**, L41 (2000).
[10] J. N. Reeves *et al.*, Nature (London) **416**, 512 (2002); Y. Krongold *et al.*, Astrophys. J. **597**, 832 (2003).
[11] D. E. Osterbrock, *Astrophysics of Gaseous Nebulae and Active Galactic Nuclei* (University Science Books, New York, 1989).
[12] N. Mott and H. S. W. Massy, *Theory of Atomic Collision* (Oxford University Press, Oxford, 1965).
[13] P. H. Norrington and I. P. Grant, J. Phys. B **20**, 4869 (1987); S. Ait-Tahar, I. P. Grant, and P. H. Norrington, Phys. Rev. A **54**, 3984 (1996).
[14] K. A. Berrington, W. Eissner, and P. H. Norrington, Comput. Phys. Commun. **92**, 290 (1995).
[15] G. X. Chen, Phys. Rev. A **76**, 062708 (2007).
[16] G. X. Chen and A. K. Pradhan, Phys. Rev. Lett. **89**, 013202 (2002); G. X. Chen, A. K. Pradhan, and W. B. Eissner, J. Phys. B **36**, 453 (2003).
[17] G. X. Chen, R. K. Smith, K. Kirby, N. S. Brickhouse, and B. J. Wargelin, Phys. Rev. A **74**, 042709 (2006).
[18] G. X. Chen and A. K. Pradhan, J. Phys. B **32**, 1809 (1999).
[19] P. L. Hagelstein and R. K. Jung, At. Data Nucl. Data Tables **37**, 121 (1987).
[20] H. L. Zhang and D. H. Sampson, At. Data Nucl. Data Tables **43**, 1 (1989).
[21] Y. K. Kim and J. P. Desclaux, Phys. Scr. **36**, 796 (1987).
[22] G. X. Chen, Phys. Rev. A **53**, 3227 (1996).
[23] K. G. Dyall, I. P. Grant, C. T. Johnson, F. A. Parpia, and E. P. Plummer, Comput. Phys. Commun. **55**, 425 (1989).
[24] GRASP2, F. A. Parpia, C. F. Fischer, and I. P. Grant (private communication). See also, F. A. Parpia, C. F. Fischer, and I. P. Grant, Comput. Phys. Commun. **94**, 249 (1996); P. Jönsson, X. He, C. F. Fischer, and I. P. Grant, *ibid.* **177**, 597 (2007).
[25] G. X. Chen and Y. B. Qiu, Phys. Rev. A **56**, 3765 (1997).
[26] G. X. Chen, P. P. Ong, and T. Lin, Chem. Phys. Lett. **289**, 428 (1998).
[27] G. X. Chen and P. P. Ong, J. Phys. B **32**, 5351 (1999).
[28] G. V. Brown, P. Beiersdorfer, D. A. Liedahl, and K. Widmann, Astrophys. J. **502**, 1015 (1998).
[29] J. M. Laming *et al.*, Astrophys. J. Lett. **545**, L161 (2000).
[30] G. V. Brown *et al.*, Phys. Rev. Lett. **96**, 253201 (2006).
[31] P. Beiersdorfer, Annu. Rev. Astron. Astrophys. **41**, 343 (2003).
[32] I. P. Grant, *Relativistic Quantum Theory of Atoms and Molecules* (Springer, Berlin, 2007).
[33] M. E. Riley and D. G. Truhlar, J. Chem. Phys. **63**, 2182 (1975).
[34] M. Mohan, R. Sharma, and W. Eissner, Astrophys. J., Suppl. Ser. **108**, 389 (1997).